

# We are IntechOpen, the world's leading publisher of Open Access books Built by scientists, for scientists

6,900

Open access books available

186,000

International authors and editors

200M

Downloads

Our authors are among the

154

Countries delivered to

TOP 1%

most cited scientists

12.2%

Contributors from top 500 universities



WEB OF SCIENCE™

Selection of our books indexed in the Book Citation Index  
in Web of Science™ Core Collection (BKCI)

Interested in publishing with us?  
Contact [book.department@intechopen.com](mailto:book.department@intechopen.com)

Numbers displayed above are based on latest data collected.  
For more information visit [www.intechopen.com](http://www.intechopen.com)



# Photorefractive Ferroelectric Liquid Crystals

Takeo Sasaki  
Tokyo University of Science  
Japan

## 1. Introduction

The photorefractive effect is one of the phenomena that can form hologram images in a material. Currently, 3D displays are expected to be widely used as next generation displays. However, current 3D displays are basically stereograms. Holographic displays that can realize natural 3D images that can be seen by the naked eye are anticipated. The photorefractive effect is a phenomenon wherein a change in the refractive index is induced by a combined mechanism of photovoltaic and electro-optic effects. A transparent material that exhibits both photovoltaic and electro-optic effects can potentially be used as a photorefractive material. The interference of two laser beams in a photorefractive material establishes a refractive index grating (**Figure 1**). When two laser beams interfere in an organic photorefractive material, charge generation occurs at the bright positions of the interference fringes. The generated charges diffuse or drift within the material. Since the mobilities of positive and negative charges are different in most organic materials, a charge separated state is formed. The charge with higher mobility diffuses over a longer distance than the charge with lower mobility, so that while the low mobility charge stays in the bright areas, the high mobility charge moves to the dark areas. The bright and dark positions of the interference fringes are thus charged with opposite polarities, and an internal electric field (space charge field) is generated in the area between the bright and dark positions. The refractive index of this area between the bright and dark positions is changed through the electro-optic effect. Thus, a refractive index grating (or hologram) is formed. One material class that exhibits high photorefractivity is glassy photoconductive polymers doped with high concentrations of D- $\pi$ -A chromophores (in which donor and acceptor groups are attached to a  $\pi$ -conjugate system). In order to obtain photorefractivity in polymer materials, a high electric field of 10–50 V/ $\mu\text{m}$  is usually applied to a polymer film. This electric field is necessary to increase the charge generation efficiency.

The photorefractive effect has been reported in surface-stabilized ferroelectric liquid crystals (SS-FLCs) doped with a photoconductive compound. Liquid crystals are classified into several groups. The most well known are nematic liquid crystals and smectic liquid crystals (**Figure 2**). Nematic liquid crystals are used in LC displays. On the other hand, smectic liquid crystals are very viscous and hence are not utilized in any practical applications. Ferroelectric liquid crystals (FLCs) belong to the class of smectic liquid crystals that have a layered structure. The molecular structure of a typical FLC contains a chiral unit, a carbonyl group, a central core, which is a rigid rod-like structure such as biphenyl, phenylpyrimidine, phenylbenzoate, and a flexible alkyl chain (**Figure 3**).

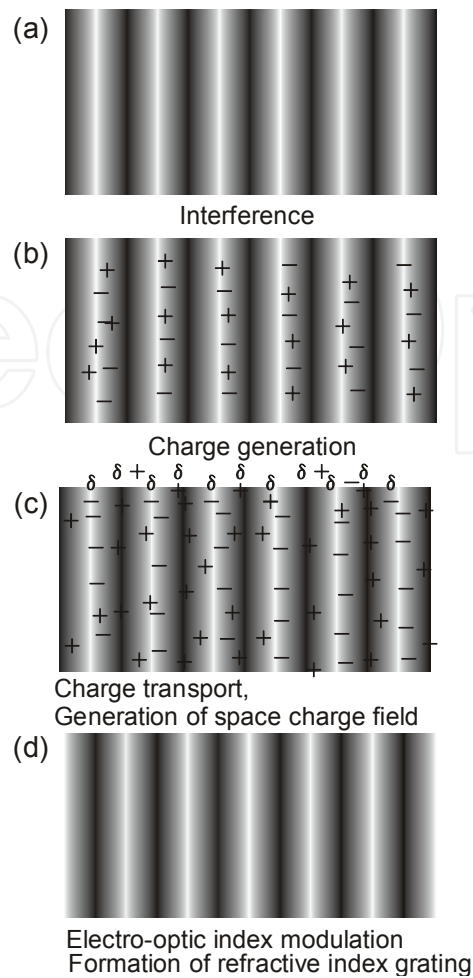


Fig. 1. Schematic illustration of the mechanism of the photorefractive effect. (a) Two laser beams interfere in the photorefractive material; (b) charge generation occurs at the light areas of the interference fringes; (c) electrons are trapped at the trap sites in the light areas, holes migrate by diffusion or drift in the presence of an external electric field and generate an internal electric field between the light and dark positions; (d) the refractive index of the corresponding area is altered by the internal electric field generated.

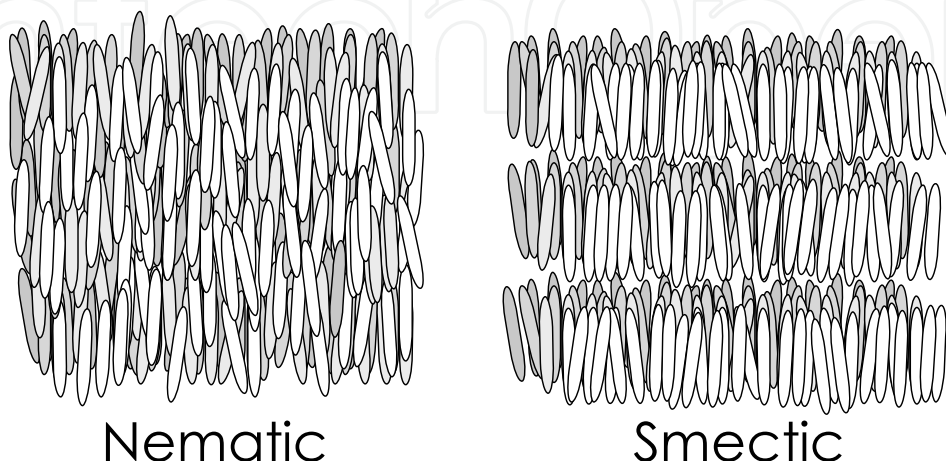


Fig. 2. Structures of the nematic and smectic phase.

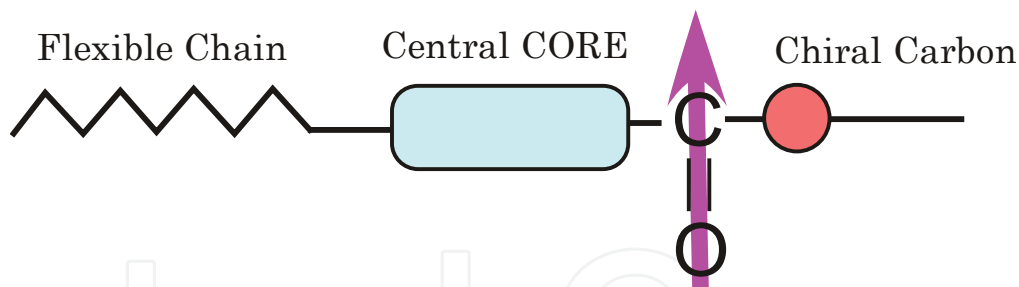
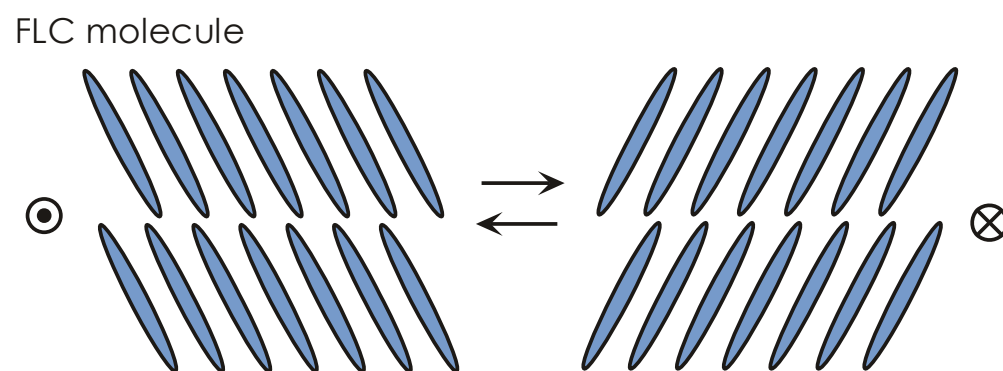


Fig. 3. Molecular structure of ferroelectric liquid crystals.

Thus, the dipole moment of a FLC molecule is perpendicular to the molecular long axis. FLCs exhibit a chiral smectic C phase ( $SmC^*$ ) that possesses a helical structure. It should be mentioned here that in order to observe ferroelectricity in these materials, the ferroelectric liquid crystals must be formed into thin films. The thickness of the film must be within a few micrometers. When an FLC is sandwiched between glass plates to form a film a few micrometers thick, the helical structure of the smectic C phase uncoils and a surface-stabilized state (SS-state) is formed in which spontaneous polarization ( $P_s$ ) appears (Figure 4).



## Electro-optic effect in FLCs

Fig. 4. Electro-optical switching in the surface-stabilized state of FLCs.

For display applications, the thickness of the film is usually  $2\ \mu\text{m}$ . In such thin films, FLC molecules can align only in two directions. This state is called a surface-stabilized state (SS-state). The alignment direction of the FLC molecules changes according to the direction of the spontaneous polarization. The direction of the spontaneous polarization is governed by the photoinduced internal electric field, giving rise to a refractive index grating with properties dependent on the direction of polarization. Figure 5 shows a schematic illustration of the mechanism of the photorefractive effect in FLCs. When laser beams interfere in a mixture of an FLC and a photoconductive compound, charge separation occurs between bright and dark positions and an internal electric field is produced. The internal electric field alters the direction of spontaneous polarization in the area between the bright and dark positions of the interference fringes, which induces a periodic change in the orientation of the FLC molecules. This is different from the processes that occur in other photorefractive materials in that the molecular dipole rather than the bulk polarization responds to the internal electric field. Since the switching of FLC molecules is due to the response of bulk polarization, the switching is extremely fast.

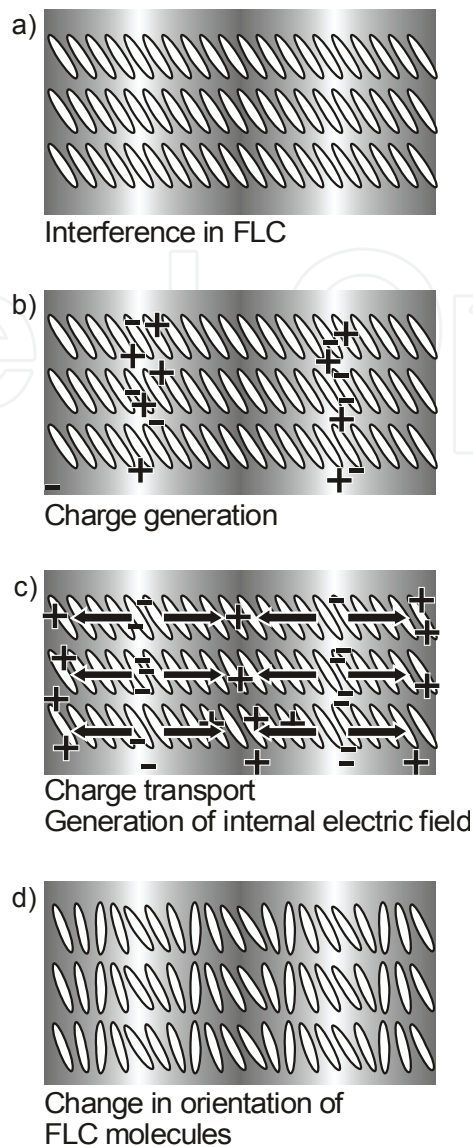


Fig. 5. Schematic illustration of the mechanism of the photorefractive effect in FLCs. (a) Two laser beams interfere in the surface-stabilized state of the FLC/photoconductive compound mixture; (b) charge generation occurs at the bright areas of the interference fringes; (c) electrons are trapped at the trap sites in the bright areas, holes migrate by diffusion or drift in the presence of an external electric field to generate an internal electric field between the bright and dark positions; (d) the orientation of the spontaneous polarization vector (i.e., orientation of mesogens in the FLCs) is altered by the internal electric field.

## 2. Characteristics of the photorefractive effect

Since a change in the refractive index via the photorefractive effect occurs in the areas between the bright and dark positions of the interference fringe, the phase of the resulting index grating is shifted from the interference fringe. This is characteristic of the photorefractive effect that the phase of the refractive index grating is  $\pi/2$ -shifted from the interference fringe. When the material is photochemically active and is not photorefractive, a photochemical reaction takes place at the bright areas, and a refractive index grating with the same phase as that of the interference fringe is formed (**Figure 6(a)**).

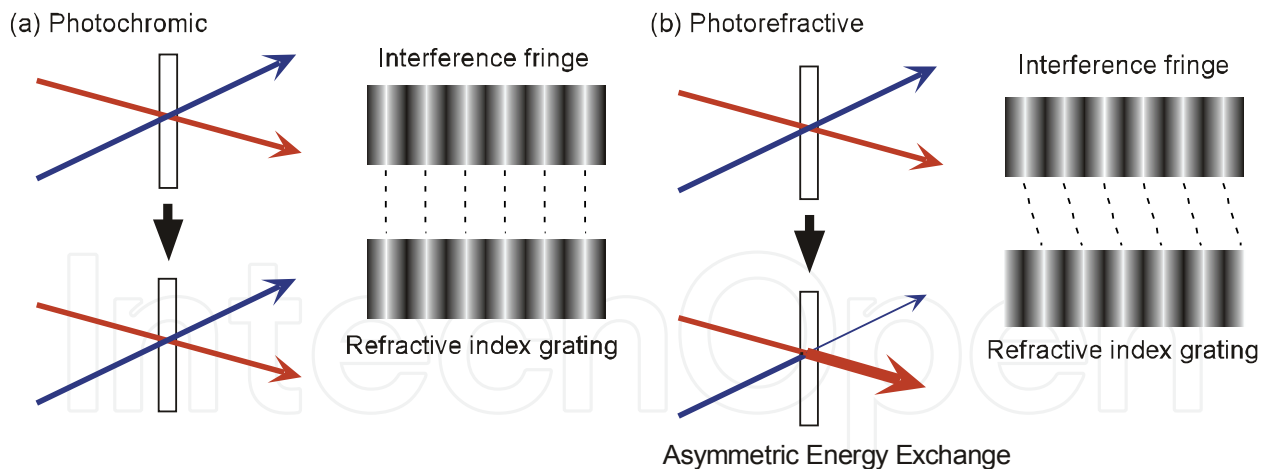


Fig. 6. (a) Photochromic grating, and (b) photorefractive grating.

The interfering laser beams are diffracted by this grating, however, the apparent transmitted intensities of the laser beams do not change because the diffraction is symmetric. Beam 1 is diffracted in the direction of beam 2 and beam 2 is diffracted in the direction of beam 1. However, if the material is photorefractive, the phase of the refractive index grating is shifted from that of the interference fringes, and this affects the propagation of the two beams. Beam 1 is energetically coupled with beam 2 for the two laser beams. Consequently, the apparent transmitted intensity of beam 1 increases and that of beam 2 decreases (**Figure 6(b)**). This phenomenon is termed asymmetric energy exchange in the two-beam coupling experiment. The photorefractivity of a material is confirmed by the occurrence of this asymmetric energy exchange.

### 3. Measurement of photorefractivity

The photorefractive effect is evaluated by a two-beam coupling method and also by a four-wave mixing experiment. **Figure 7 (a)** shows a schematic illustration of the experimental setup used for the two-beam coupling method. A p-polarized beam from a laser is divided into two beams by a beam splitter, and the beams are interfered within the sample film.

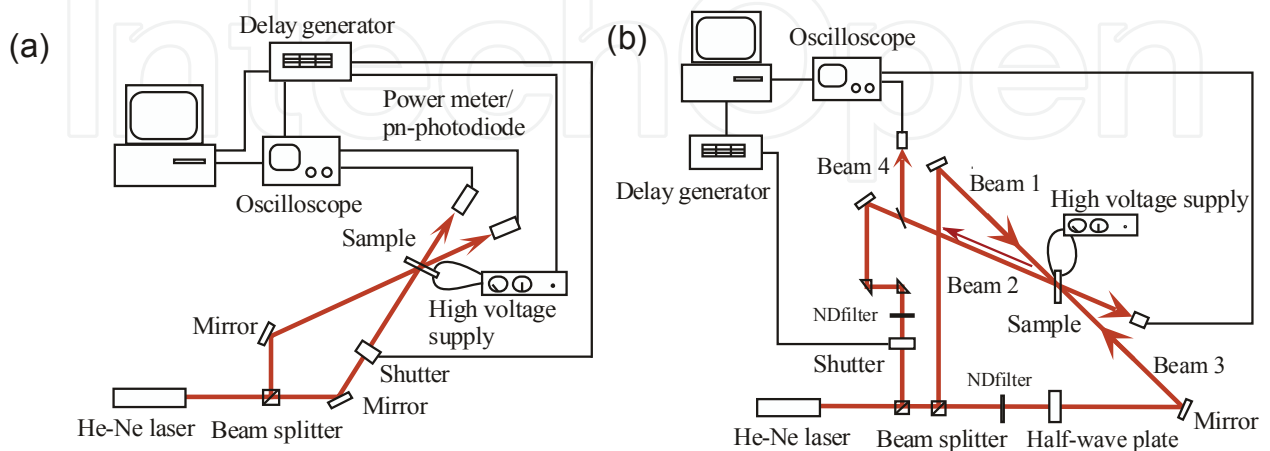


Fig. 7. Schematic illustrations of the experimental set-up for the (a) two-beam coupling, and (b) four-wave-mixing techniques.

An electric field is applied to the sample using a high voltage supply unit. This external electric field is applied in order to increase the efficiency of charge generation in the film. The change in the transmitted beam intensity is monitored. If a material is photorefractive, an asymmetric energy exchange is observed. The magnitude of photorefractivity is evaluated using a parameter called the gain coefficient, which is calculated from the change in the transmitted intensity of the laser beams induced through the two-beam coupling. In order to calculate the two-beam coupling gain coefficient, it must be determined whether the diffraction condition is in the Bragg regime or in the Raman-Nath regime. These diffraction conditions are distinguished by a dimensionless parameter  $Q$ .

$$Q = 2\pi\lambda L / n\Lambda^2 \quad (1)$$

$Q > 1$  is defined as the Bragg regime of optical diffraction. In this regime, multiple scattering is not permitted, and only one order of diffraction is produced. Conversely,  $Q < 1$  is defined as the Raman-Nath regime of optical diffraction. In this regime, many orders of diffraction can be observed. Usually,  $Q > 10$  is required to guarantee that the diffraction is entirely in the Bragg regime. When the diffraction is in the Bragg diffraction regime, the two-beam coupling gain coefficient  $\Gamma$  ( $\text{cm}^{-1}$ ) is calculated according to the following equation:

$$\Gamma = \frac{1}{D} \ln \left( \frac{gm}{1+m-g} \right) \quad (2)$$

where  $D = L / \cos(\theta)$  is the interaction path for the signal beam ( $L$  = sample thickness,  $\theta$  = propagation angle of the signal beam in the sample),  $g$  is the ratio of the intensities of the signal beam behind the sample with and without a pump beam, and  $m$  is the ratio of the beam intensities (pump/signal) in front of the sample.

A schematic illustration of the experimental setup used for the four-wave mixing experiment is shown in **Figure 7 (b)**. S-polarized writing beams are interfered in the sample film and the diffraction of a p-polarized probe beam, counter-propagating to one of the writing beams, is measured. The diffracted beam intensity is typically measured as a function of time, applied (external) electric field, writing beam intensities, etc. The diffraction efficiency is defined as the ratio of the intensity of the diffracted beam and the intensity of the probe beam that is transmitted when no grating is present in the sample due to the writing beams. In probing the grating, it is important that beam 3 does not affect the grating or interact with the writing beams. This can be ensured by making the probe beam much weaker than the writing beams, and by having the probe beam polarized orthogonal to the writing beams.

## 4. Photorefractive effect of FLCs

### 4.1 Two-beam coupling experiments on FLCs

The photorefractive effect in an FLC was first reported by Wasielewsky et al. in 2000. Since then, details of photorefractivity in FLC materials have been further investigated by Sasaki et al. and Golemme et al. The photorefractive effect in a mixture of an FLC and a photoconductive compound was measured in a two-beam coupling experiment using a 488 nm  $\text{Ar}^+$  laser. The structures of the photoconductive compounds used are shown in **Figure 8**. A commercially available FLC, SCE8 (Clariant), was used. CDH was used as a

photoconductive compound, and TNF was used as a sensitizer. The concentrations of CDH and TNF were 2 wt% and 0.1 wt% respectively. The samples were injected into a 10- $\mu\text{m}$ -gap glass cell equipped with 1 cm<sup>2</sup> ITO electrodes and a polyimide alignment layer (**Figure 9**).

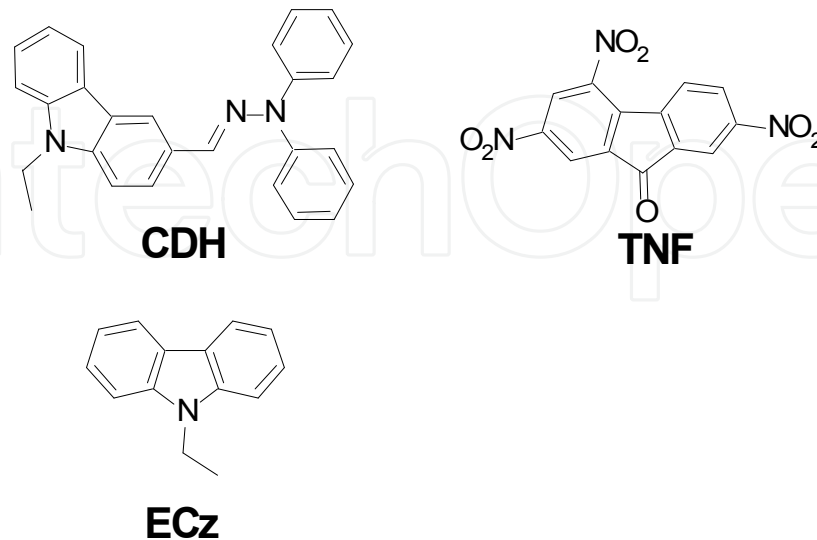


Fig. 8. Structures of the photoconductive compound CDH, ECz and the sensitizer TNF

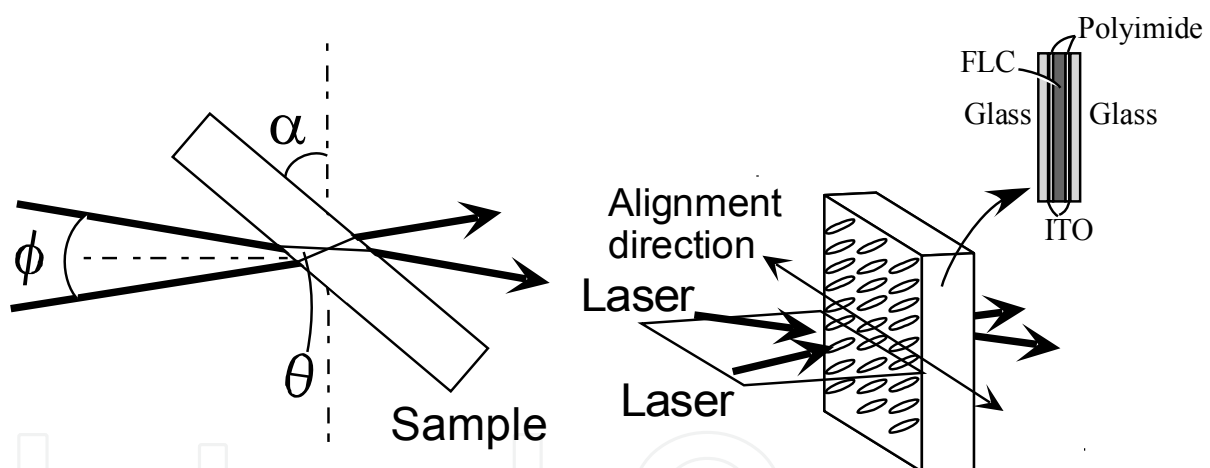


Fig. 9. Laser beam incidence condition and the structure of the LC cell.

**Figure 10** shows a typical example of asymmetric energy exchange observed in the FLC(SCE8)/CDH/TNF sample under an applied DC electric field of 0.1 V/ $\mu\text{m}$ . Interference of the divided beams in the sample resulted in increased transmittance of one beam and decreased transmittance of the other. The change in the transmitted intensities of the two beams is completely symmetric, as can be seen in **Figure 10**. This indicates that the phase of the refractive index grating is shifted from that of the interference fringes. The grating formation was within the Bragg diffraction regime, and no higher order diffraction was observed under the conditions used.

The temperature dependence of the gain coefficient of SCE8 doped with 2 wt% CDH and 0.1 wt% TNF is shown in **Figure 11 (a)**. Asymmetric energy exchange was observed only at temperatures below 46°C. The spontaneous polarization of the identical sample is plotted as a function of temperature in **Figure 11 (b)**.

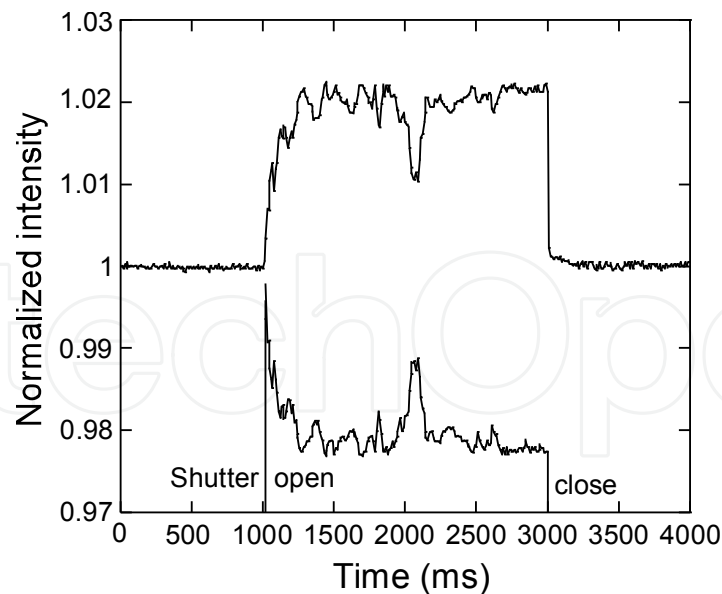


Fig. 10. Typical example of asymmetric energy exchange observed in an FLC (SCE8) mixed with 2 wt% CDH and 0.1 wt% TNF. An electric field of  $+0.3 \text{ V}/\mu\text{m}$  was applied to the sample.

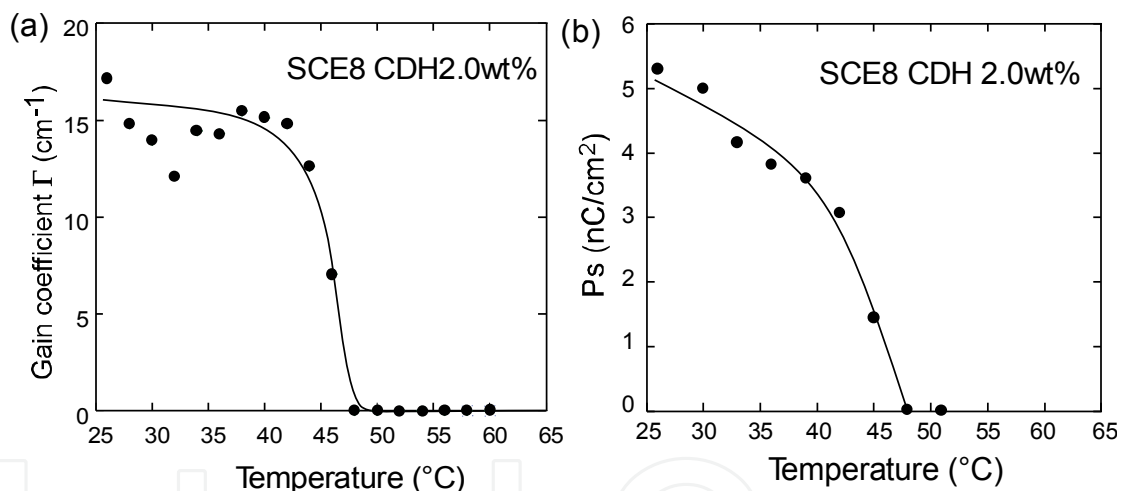


Fig. 11. Temperature dependence of (a) gain coefficient and (b) spontaneous polarization of an FLC (SCE8) mixed with 2 wt% CDH and 0.1 wt% TNF. For two-beam coupling experiments, an electric field of  $0.1 \text{ V}/\mu\text{m}$  was applied to the sample.

Similarly, the spontaneous polarization vanished when the temperature was raised above  $46^\circ\text{C}$ . Thus, asymmetric energy exchange was observed only in the temperature range in which the sample exhibits ferroelectric properties, in other words, the  $\text{SmC}^*$  phase. Since the molecular dipole moment of the FLCs is small and the dipole moment is aligned perpendicular to the molecular axis, large changes in the orientation of the molecular axis cannot be induced by an internal electric field in the  $\text{SmA}$  or  $\text{N}^*$  phase of the FLCs. However, in the  $\text{SmC}^*$  phase, reorientation associated with spontaneous polarization occurs due to the internal electric field. The spontaneous polarization also causes orientation of FLC molecules in the corresponding area to change accordingly. A maximum resolution of  $0.8 \mu\text{m}$  was obtained in this sample.

FLC	Ps at 25 °C (nC/cm <sup>2</sup> )	Phase transition temperature <sup>a</sup> (°C)	Response time $\tau^b$ ( $\mu$ s)	Rotational viscosity $\gamma_\phi$ (mPas)	Tilt angle (deg.)
015/000	9	- SmC* 71 SmA 83 N* 86 I	70	60	24
015/100	33	- SmC* 72 SmA 83 N* 86 I	21	80	23
016/000	-4.3	- SmC* 72 SmA 85 N* 93 I	70	61	25
016/030	-5.9	- SmC* 72 SmA 85 N* 93 I	47	82	25
016/100	-10.5	- SmC* 72 SmA 85 N* 94 I	20	60	27
017/000	9.5	- SmC* 70 SmA 76 N* 87 I	93	47	26
017/100	47	- SmC* 73 SmA 77 N* 87 I	23	116	27
018/000	23	- SmC* 65 SmA 82 N* 88 I	59	68	22
018/100	40	- SmC* 67 SmA 82 N* 89 I	30	97	23
019/000	8.3	- SmC* 60 SmA 76 N* 82 I	262	37	19
019/100	39	- SmC* 64 SmA 78 N* 87 I	53	75	20
SCE8	-4.5	- SmC* 60 SmA 80 N* 104 I	50	76	20
M4851/000	-4.0	- SmC* 64 SmA 69 N* 73 I	40	-	25
M4851/050	-14	- SmC* 65 SmA 70 N* 74 I	22	65	28

<sup>a</sup> C, crystal; SmC\*, chiral smectic C phase; SmA, smectic A phase; N\* chiral nematic phase; I, isotropic phase

<sup>b</sup> Response time to a 10 V/ $\mu$ m electric field at 25 °C in a 2- $\mu$ m cell.

Table 1. Physical properties of the FLCs investigated

#### 4.2 Comparison of photorefractive properties of FLCs

The photorefractive properties of a series of FLCs with different properties were investigated. The properties of the FLCs are shown in **Table 1**. Unfortunately, the chemical structures of these FLCs are not exhibited. All the FLCs listed in **Table 1** exhibited finely aligned SS-states when they were not mixed with photoconductive compounds (CDH and TNF). **Figure 12** shows typical examples of the textures observed in the 017/000, M4851/050 and SCE8 FLCs.

As the CDH concentration increased, defects appeared in the texture. The M4851/050 and SCE8 FLCs retained the SS-state with few defects for CDH concentrations below 2 wt%. All the FLCs listed in **Table 1**, except for SCE8 and M4851/050, exhibited distorted SS-states, and light scattering was very strong when mixed with CDH at concentrations higher than 0.5 wt%. The SCE8 and M4851/050 FLCs displayed finely aligned SS-state domains in a 10  $\mu$ m-gap cell and exhibited asymmetric energy exchange. FLCs that formed an SS-state with many defects did not exhibit clear asymmetric energy exchange. In these distorted SS-states, the laser beams are strongly scattered, precluding the formation of a refractive index grating.

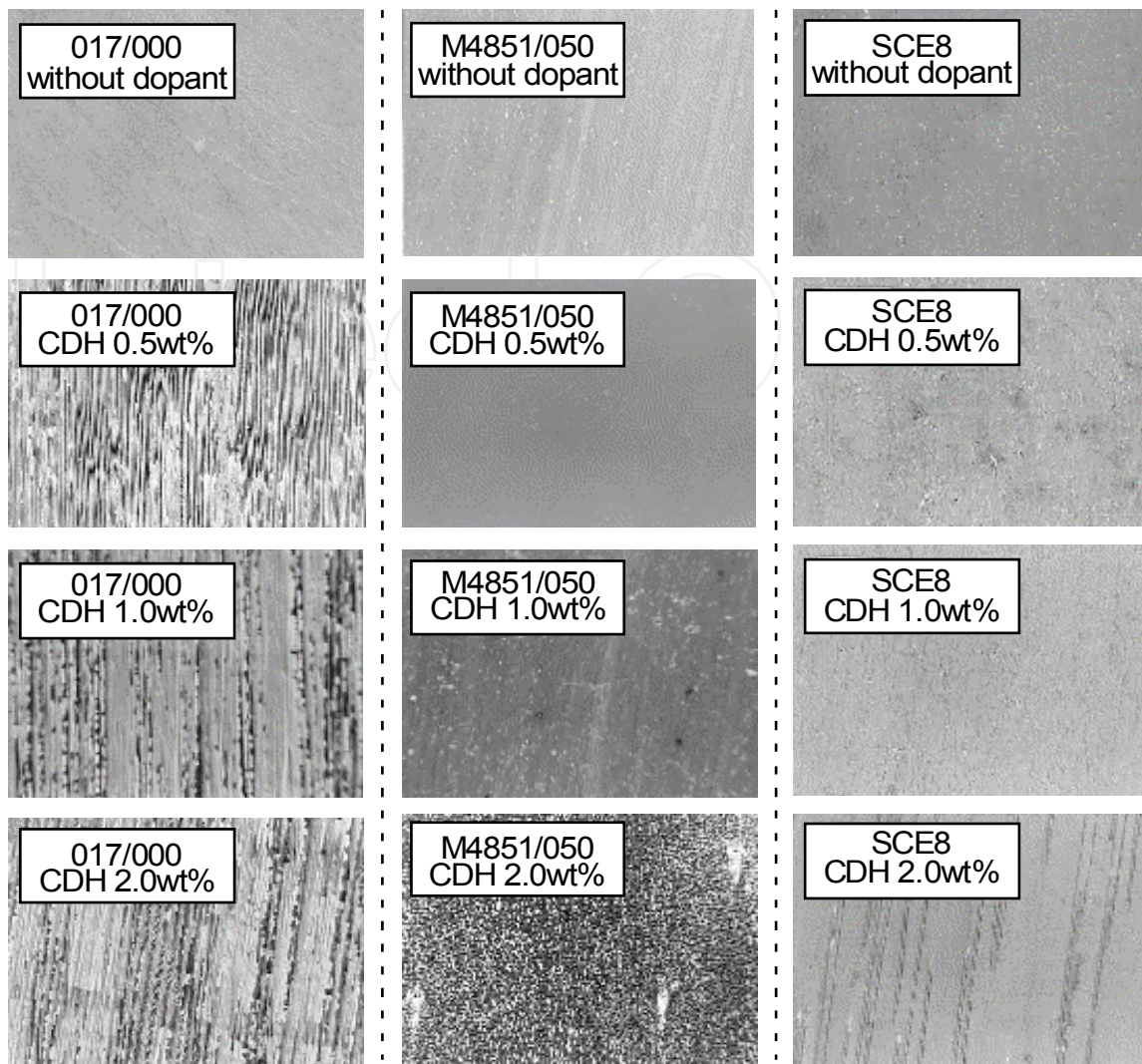


Fig. 12. Textures observed by POM observation of SS-states in FLCs.

#### 4.3 Effect of the magnitude of the applied electric field

In polymeric photorefractive materials, the strength of the externally applied electric field is a very important factor. The external electric field is necessary to increase the charge separation efficiency sufficiently to induce a photorefractive effect. In other words, photorefractivity of the polymer is obtained only with application of a few  $V/\mu\text{m}$  electric field.<sup>3-5</sup> The thickness of the polymeric photorefractive material commonly reported is about  $100\ \mu\text{m}$ , so the voltage necessary to induce the photorefractive effect is a few kV. On the other hand, the photorefractive effect in FLCs can be induced by applying a very weak external electric field. The maximum gain coefficient for the FLC (SCE8) sample was obtained using an electric field strength of only  $0.2\text{--}0.4\ V/\mu\text{m}$ . The thickness of the FLC sample is typically  $10\ \mu\text{m}$ , so that the voltage necessary to induce the photorefractive effect is only a few V. The dependence of the gain coefficient of a mixture of FLC (SCE8)/CDH/TNF on the strength of the electric field is shown in **Figure 13**. The gain coefficient of SCE8 doped with  $0.5\text{--}1\ \text{wt}\%$  CDH increased with the strength of the external electric field. However, the gain coefficient of SCE8 doped with  $2\ \text{wt}\%$  CDH decreased when the external electric field exceeded  $0.4\ V/\mu\text{m}$ . The same tendency was observed for

M4851/050 as well. The formation of an orientational grating is enhanced when the external electric field is increased from 0 to 0.2 V/ $\mu\text{m}$  as a result of induced charge separation under a higher external electric field. However, when the external electric field exceeded 0.2 V/ $\mu\text{m}$ , a number of zig-zag defects appeared in the surface-stabilized state. These defects cause light scattering and result in a decrease in the gain coefficient.

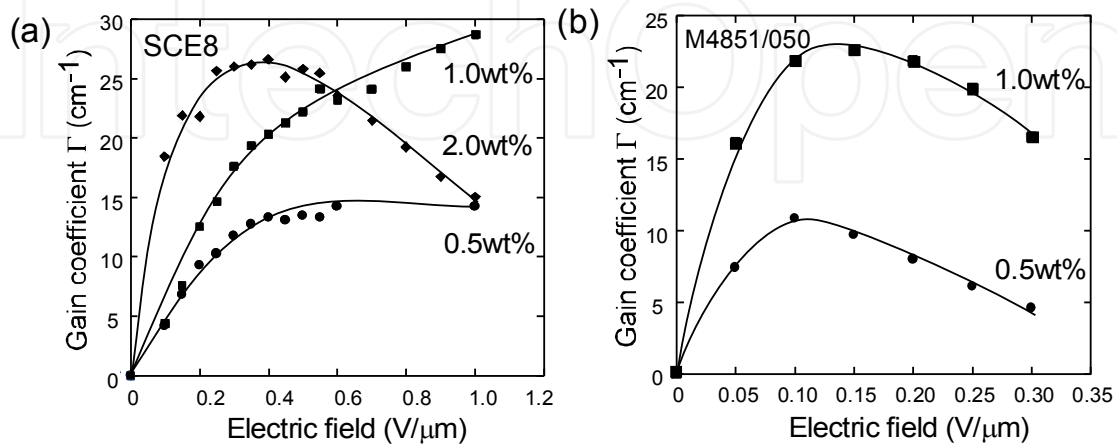


Fig. 13. Electric field dependence of the gain coefficient of SCE8 and M4851/050 mixed with several concentrations of CDH and 0.1 wt% TNF in a 10  $\mu\text{m}$ -gap cell measured at 30 °C.

#### 4.4 Refractive index grating formation time

The formation of a refractive index grating involves charge separation and reorientation. The index grating formation time is affected by these two processes, and both may be rate-determining steps. The refractive index grating formation times in SCE8 and M4851/050 were determined based on the simplest single-carrier model of photorefractivity, wherein the gain transient is exponential. The rising signal of the diffracted beam was fitted using a single exponential function, shown in equation (3).

$$\gamma(t) - 1 = (\gamma - 1)[1 - \exp(-t/\tau)]^2 \quad (3)$$

Here,  $\gamma(t)$  represents the transmitted beam intensity at time  $t$  divided by the initial intensity ( $\gamma(t) = I(t)/I_0$ ) and  $\tau$  is the formation time. The grating formation time in SCE8/CDH/TNF is plotted as a function of the strength of the external electric field in **Figure 14 (a)**. The grating formation time decreased with increasing electric field strength due to the increased efficiency of charge generation. The formation time was shorter at higher temperatures, corresponding to a decrease in the viscosity of the FLC with increasing temperature. The formation time for SCE8 was found to be 20 ms at 30°C. As shown in **Figure 14 (b)**, the formation time for M4851/050 was found to be independent of the magnitude of the external electric field, with a time of 80-90 ms for M4851/050 doped with 1 wt% CDH and 0.1 wt% TNF. This is slower than for SCE8, although the spontaneous polarization of M4851/050 (-14 nC/cm<sup>2</sup>) is larger than that of SCE8 (-4.5 nC/cm<sup>2</sup>), and the response time of the electro-optical switching (the flipping of spontaneous polarization) to an electric field ( $\pm 10$  V in a 2  $\mu\text{m}$  cell) is shorter for M4851/050. The slower formation of the refractive index grating in M4851/050 is likely due to the poor homogeneity of the SS-state and charge mobility.

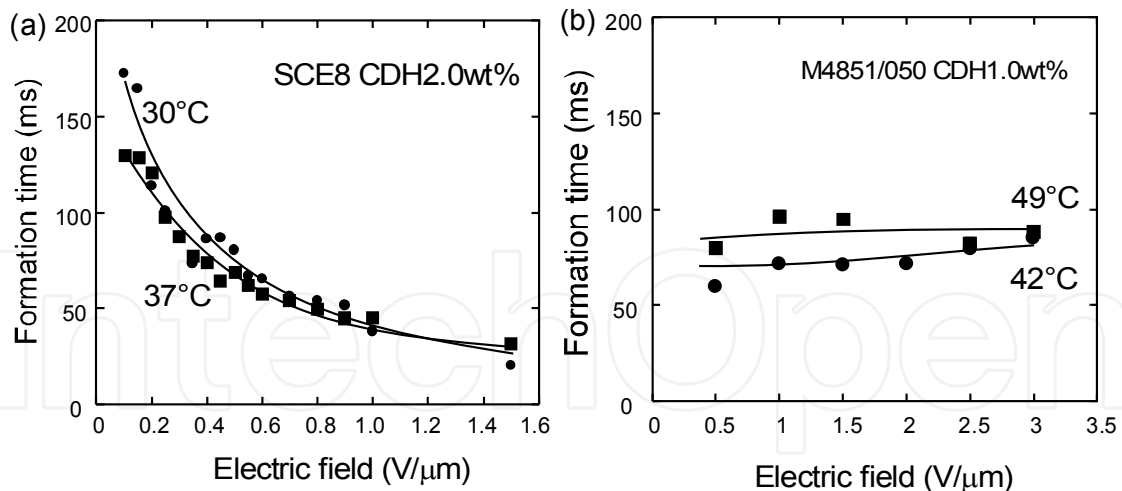


Fig. 14. Electric field dependence of the index grating formation time. (a) SCE8 mixed with 2 wt% CDH and 0.1 wt% TNF in the two-beam coupling experiment. ●, measured at 30 °C ( $T/T_{SmC^*-SmA}=0.95$ ); ■, measured at 36 °C ( $T/T_{SmC^*-SmA}=0.97$ ). (b) M4851/050 mixed with 1 wt% CDH and 0.1 wt% TNF in a two-beam coupling experiment. ●, measured at 42 °C ( $T/T_{SmC^*-SmA}=0.95$ ); ■, measured at 49 °C ( $T/T_{SmC^*-SmA}=0.97$ ).

#### 4.5 Formation mechanism of the internal electric field in FLCs

Since the photorefractive effect is induced by the photoinduced internal electric field, the mechanism of the formation of the space-charge field in the FLC medium is important. The two-beam coupling gain coefficients of mixtures of FLC (SCE8) and photoconductive compounds under a DC field were investigated as a function of the concentration of TNF (electron acceptor). The photoconductive compounds, CDH, ECz and TNF (Figure 8), were used in this examination. When an electron donor with a large molecular size (CDH) relative to the TNF was used as the photoconductive compound, the gain coefficient was strongly affected by the concentration of TNF (Figure 15(a)). However, when ethylcarbazole (ECz), whose molecular size is almost the same as that of TNF, was used, the gain coefficient was less affected by the TNF concentration (Figure 15(b)).

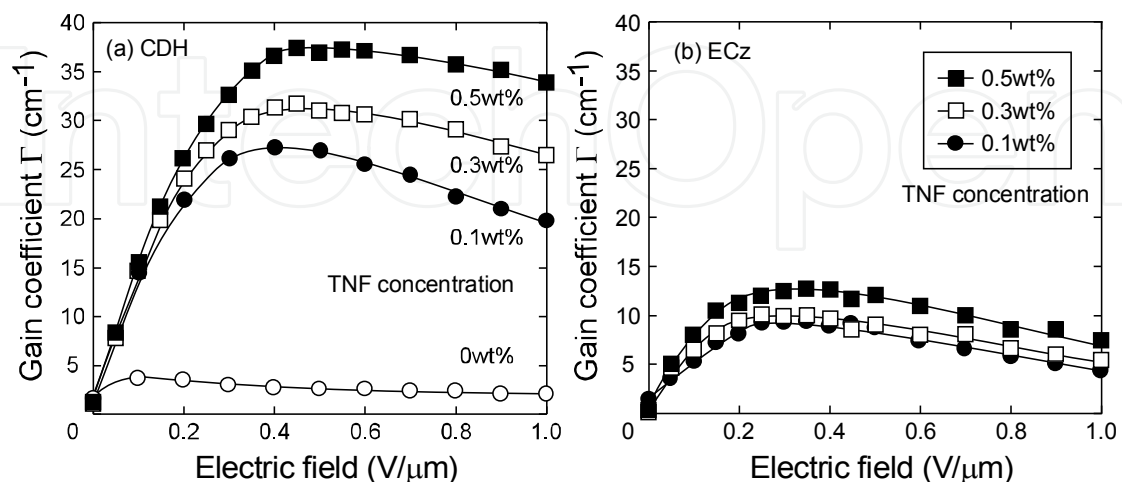


Fig. 15. Dependence of the TNF concentration on the gain coefficients of an FLC doped with photoconductive dopants. (a) SCE8 doped with 2 wt% CDH, (b) SCE8 doped with 2 wt% ECz. An electric field of  $\pm 0.5$  V/μm, 100 Hz was applied.

As shown in **Figure 16**, the difference in the change in absorbance at 488 nm upon addition of TNF was not significant when comparing CDH and ECz. Therefore, the results shown in **Figure 15** cannot be explained based on this difference.

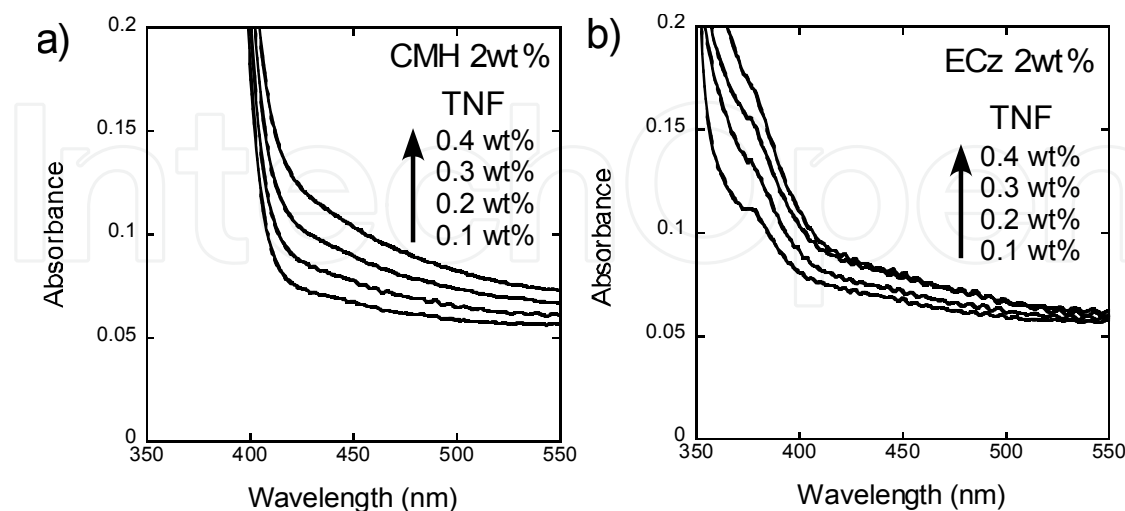


Fig. 16. Absorption spectra of mixtures of FLC (SCE8) and CDH in a 10  $\mu\text{m}$ -gap cell. The concentrations of the photoconductive compounds were fixed at 2 wt% and the TNF concentration was varied from 0 to 0.5 wt%. The reflection at the cell surface and light scattering in the LC are not subtracted.

These findings suggest that ionic conduction plays a major role in the formation of the space-charge field. The mobility of the CDH cation is smaller than that of the TNF anion, and this difference in mobility is thought to be the origin of the charge separation. In this case, the magnitude of the internal electric field is dominated by the concentration of the ionic species. On the other hand, the difference in the mobilities of ECz and TNF is small, and thus, less effective charge separation is induced, indicating that the internal electric field is independent of the concentration of ionic species.

## 4.6 Photorefractive effect in FLC mixtures containing photoconductive chiral compounds

### 4.6.1 Photoconductive chiral dopants

The photorefractive effect in FLCs was investigated using commercially available FLC mixtures until 2010 (the compositions of these FLC materials are not shown here). Compared to nematic LCs, the FLCs are more crystal than liquid, and the preparation of fine FLC films requires sophisticated techniques. Obtaining a uniformly aligned, defect-free, surface-stabilized FLC (SS-FLC) using a single FLC compound is very difficult, and mixtures of several LC compounds are usually used to obtain fine SS-FLC films. The FLC mixtures are composed of the base LC (SmC phase of the forming LC), which is also a mixture of several LC compounds and a chiral compound. The chiral compound introduces a helical structure into the LC phase through supramolecular interactions. In order to utilize an FLC as a photorefractive material, photoconductive compounds must be added to the FLC. However, the introduction of such non-LC compounds into the FLC deteriorates the formation of a uniformly aligned SS-state. Thus, adequate design of the photoconductive compounds is crucial. Sasaki et al. have synthesized chiral compounds that also show photoconductivity (photoconductive chiral dopants); these chiral compounds were

synthesized and mixed with the base LC compounds. The structures of the photoconductive chiral dopants and base LCs are shown in **Figure 17**. A photorefractive FLC material is obtained by just mixing a photoconductive chiral dopant with the base LC.

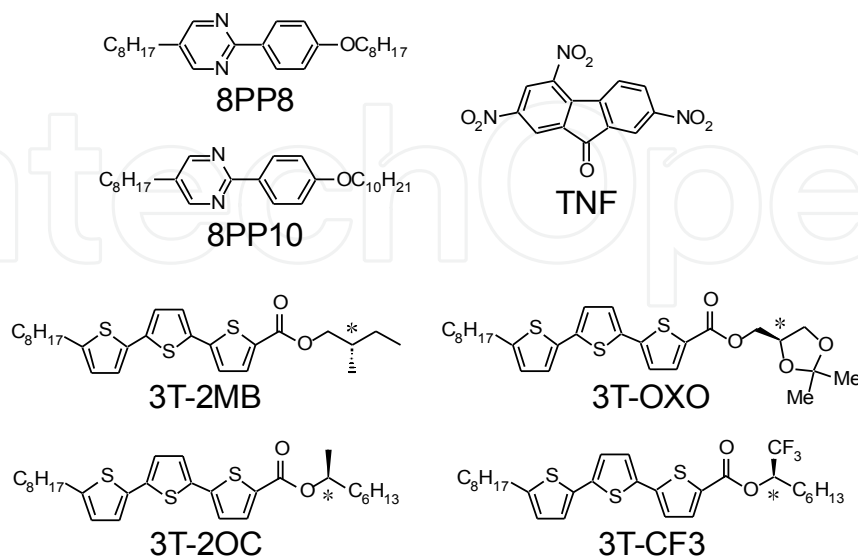


Fig. 17. Structures of the smectic LCs (8PP8 and 8PP10), photoconductive chiral dopants (3T-2MB, 3T-2OC, 3T-OXO and 3T-CF3) and the sensitizer TNF used in this work.

#### 4.6.2 Ferroelectricity and photoconductivity of the FLC mixture

The base LC, which is a 1:1 mixture of 8PP8 and 8PP10, was mixed with the photoconductive chiral dopant and the electron acceptor, which is TNF in this case. The concentration of TNF was set to 0.1 wt%. The phase diagrams of the base LC, TNF, and chiral dopants are shown in **Figure 18**.

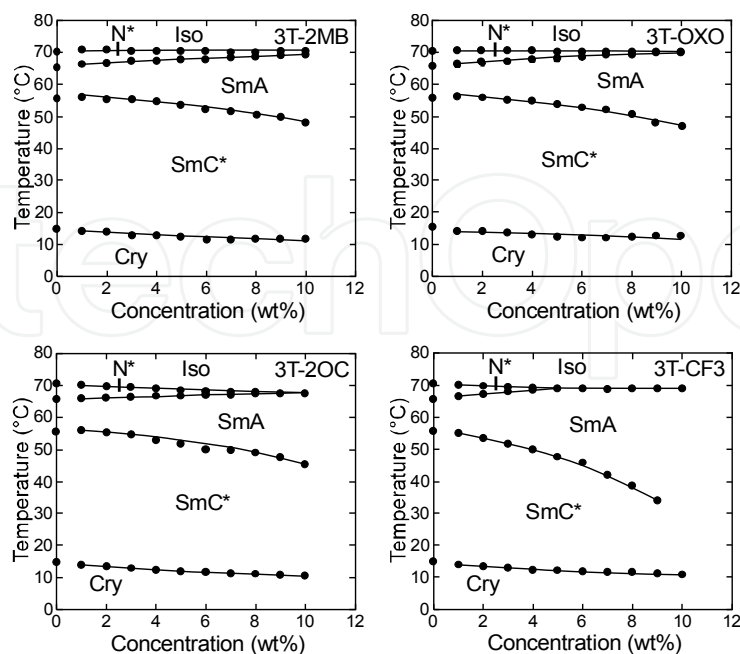


Fig. 18. Phase diagrams of mixtures of the base LC and chiral compounds. The concentration of TNF was set to 0.1 wt%.

The terthiophene chiral dopant used in this study had high miscibility with the phenyl pyrimidine-type smectic LC. The chiral smectic C (SmC\*) phase appeared in all mixtures of the base LC and chiral dopants used in this study. With increasing concentration of the chiral dopants, the temperature range of the SmC\* phase and the chiral nematic (N\*) phase was reduced, whereas that of the smectic A (SmA) phase was enhanced. The miscibility of the 3T-CF<sub>3</sub> with the base LC was the lowest among the four chiral dopants used in this study. The dipole moment of the trifluoromethyl-substituted group is large, so that the 3T-CF<sub>3</sub> molecules tended to aggregate. The magnitude of spontaneous polarization ( $P_s$ ) of the FLC mixtures (mixtures of the base LC with photoconductive dopants and TNF) was measured by the triangular waveform voltage method. A  $P_s$  flip signal observed in the triangular wave method measurement and the magnitude of the  $P_s$  as a function of the concentration of a chiral dopant are shown in **Figure 19**.

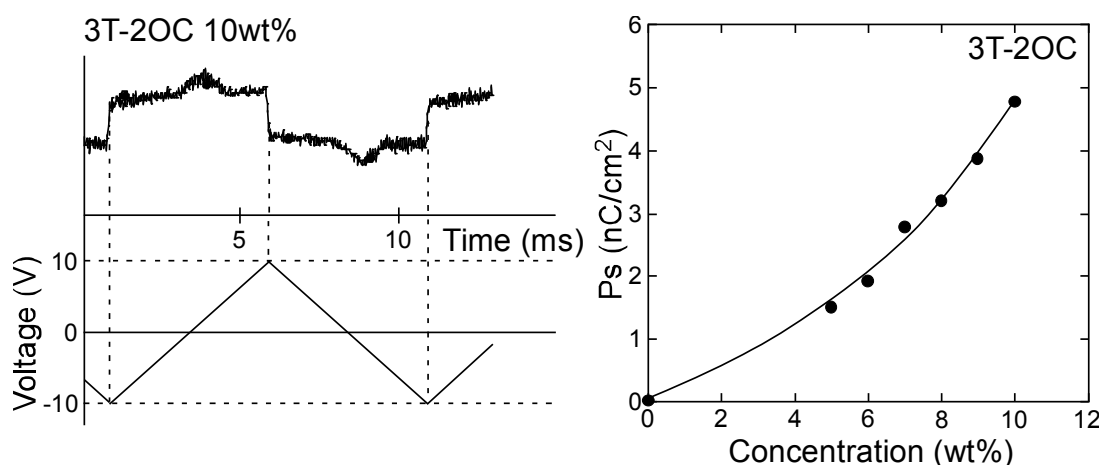


Fig. 19. Spontaneous polarization observed in mixtures of the base LC and 3T-2OC. (a) A typical example of the observed signal in the triangular waveform method. (b) Magnitude of the spontaneous polarization plotted as a function of the concentration of 3T-2OC.

The magnitude of the  $P_s$  of the mixtures of the base LC with chiral dopants was in the range of a few  $\text{nC}/\text{cm}^2$ . The mixtures of the base LC with 3T-2MB and 3T-OXO exhibited  $P_s$  values smaller than  $1 \text{ nC}/\text{cm}^2$ , which is the measurement limit of our equipment. The spontaneous polarization increased with the 3T-2OC concentration, and a  $P_s$  value of  $4.8 \text{ nC}/\text{cm}^2$  was obtained at a 10 wt% concentration. The UV-vis absorption spectra of the photoconductive chiral dopants in chloroform solutions are shown in **Figure 20**. All the samples exhibited absorption maxima at 394 nm. Absorption at 488 nm (wavelength of the laser used in this study) was small.

The small absorption at the laser wavelength is advantageous for minimizing optical loss. The photocurrents in mixtures of the base LC, photoconductive chiral dopant and TNF were measured. As shown in **Figure 21**, the samples were good insulators in the dark. When the samples were irradiated with 488 nm laser light, photocurrents were clearly observed. The magnitudes of the photocurrents were slightly different in the four samples. The only difference in the molecular structures of these compounds is the chiral substituent. Thus, this variation in the photocurrent cannot be attributed to the difference in the molecular structure. It is possible that the miscibility of the photoconductive chiral compounds in the LC and the homogeneity of the LC phase affected the magnitude of the photocurrent.

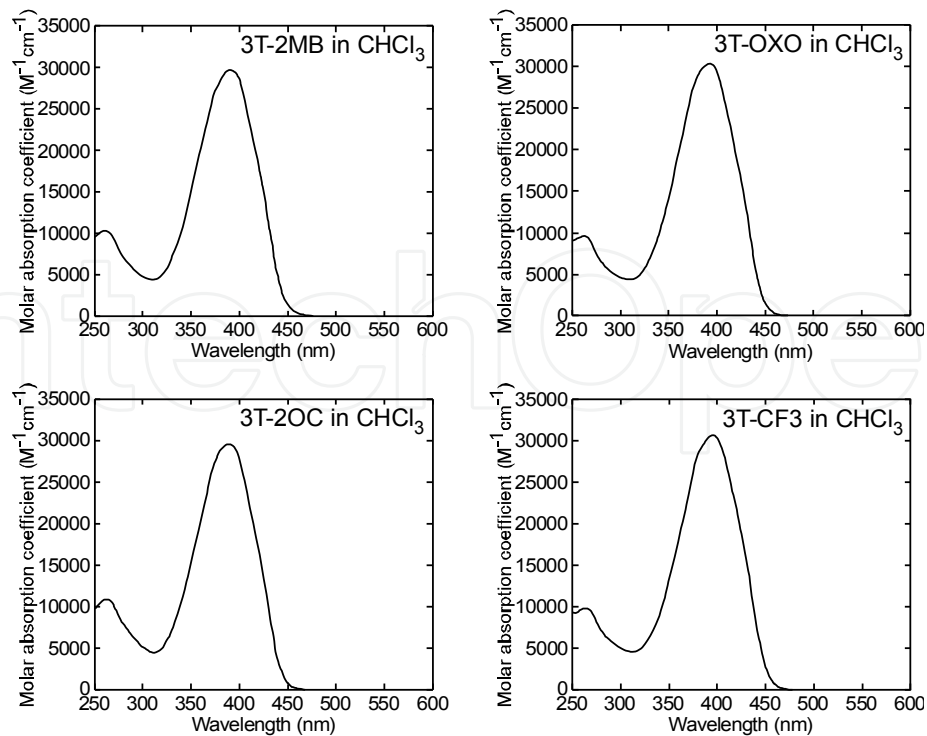


Fig. 20. Absorption spectra of chloroform solutions of the chiral compounds. (a) 3T-2MB; (b) 3T-2OC; (c) 3T-OXO; (d) 3T-CF3. The concentration of the chiral compounds was  $6.3 \times 10^{-4}$  mol/L.

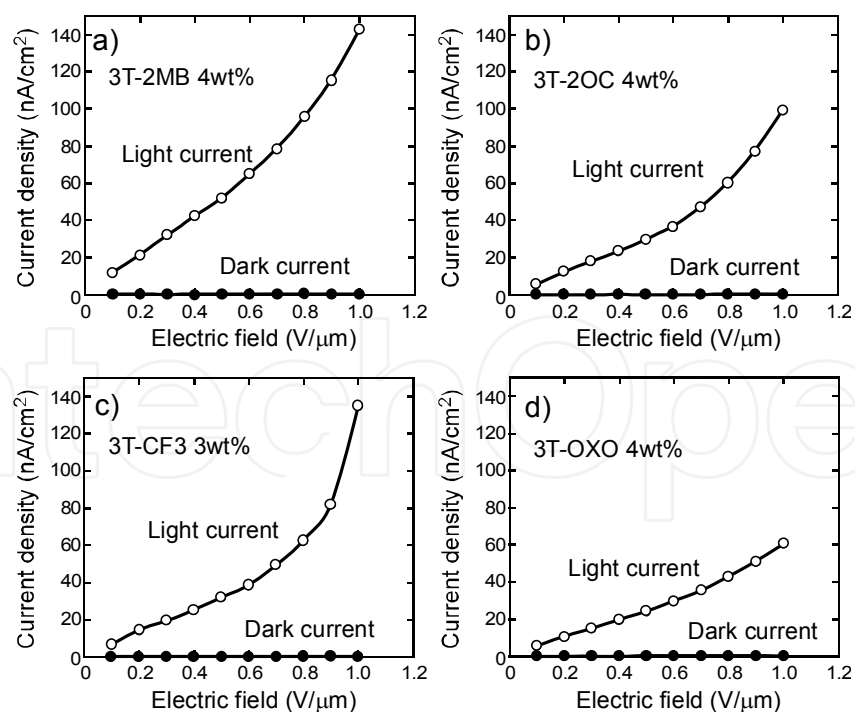


Fig. 21. Magnitudes of light-current and dark-current of mixtures of the base LC, photoconductive chiral compound and TNF measured in a 10-μm-gap LC cell as a function of the external electric field. An electric field of 0.1 V/μm was applied. A 488 nm Ar<sup>+</sup> laser (10 mW/cm<sup>2</sup>, 1 mm diameter) was used as the irradiation source.

#### 4.6.3 Two-beam coupling experiment on photoconductive FLC mixtures

The difference in the gain coefficients in mixtures of the base LC, photoconductive chiral dopant (3T-2MB, 3T-2OC, 3T-OXO, or 3T-CF3), and TNF was investigated. All the samples formed a finely aligned SS-state in 10- $\mu\text{m}$ -gap cells with a LX-1400 polyimide alignment layer and clearly exhibited photorefractivity in the ferroelectric phase. Asymmetric energy exchange was observed only in the temperature range in which the sample exhibited ferroelectric properties (SmC\* phase). The gain coefficients of the samples are plotted as a function of the magnitude of the external electric field in **Figure 22**. As the concentration of the photoconductive chiral dopant increased, so did the gain coefficient. This may be due to increased charge mobility in the FLC medium and an increase in the magnitude of Ps. All the samples exhibited relatively large photorefractivity. A gain coefficient higher than 100  $\text{cm}^{-1}$  was obtained in the 3T-2OC (6 wt%) sample with the application of an electric field of only 0.2  $\text{V}/\mu\text{m}$ . A gain coefficient higher than 100  $\text{cm}^{-1}$  was also obtained in the 3T-2MB sample at an applied electric field of 0.5  $\text{V}/\mu\text{m}$ . In order to obtain photorefractivity in polymer materials, the application of a high electric field in the range of 10–50  $\text{V}/\mu\text{m}$  to the polymer film is typically required. The small electric field necessary for activating the photorefractive effect in FLCs is thus a great advantage for photorefractive devices. The grating formation time in the mixtures of the base LC, photoconductive chiral dopant and TNF is plotted as a function of the strength of the external electric field in **Figure 23**.

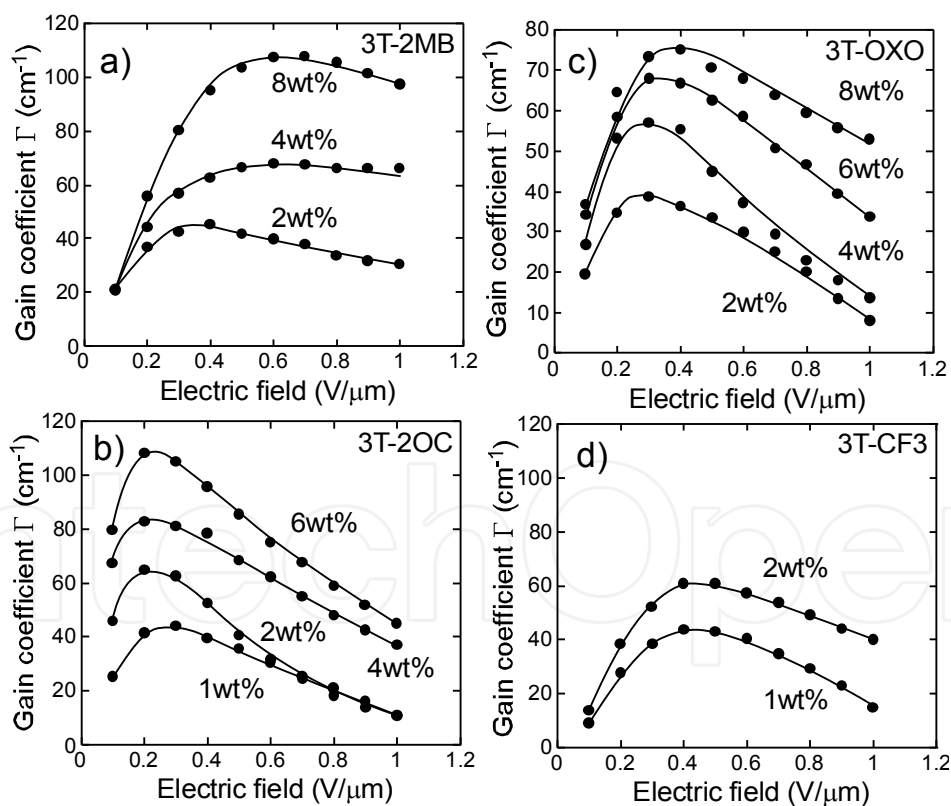


Fig. 22. Electric field dependence of the gain coefficients of the mixtures of the base LC, photoconductive chiral compounds, and TNF. (a) 3T-2MB; (b) 3T-2OC; (c) 3T-OXO; (d) 3T-CF3.

The grating formation time decreased with increasing electric field strength due to the increased efficiency of charge generation. The shortest formation time was obtained to be 5–

8 ms at 1 V/ $\mu\text{m}$  external electric field for all the chiral compounds. The 3T-CF3 sample exhibited the fastest response, because of the larger polarity of 3T-CF3.

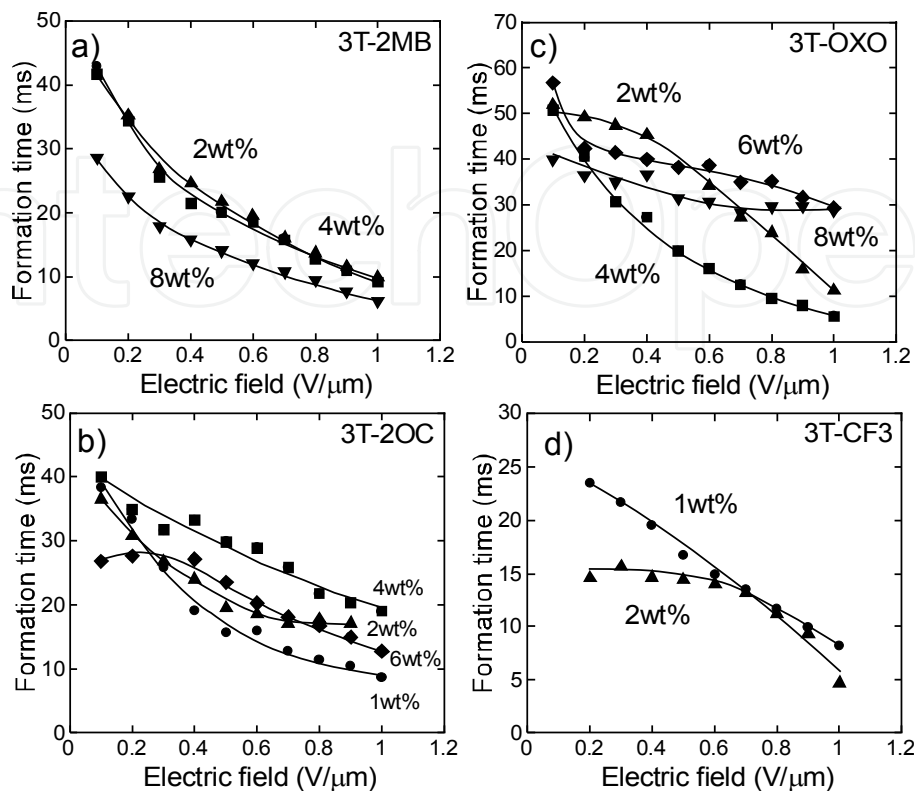


Fig. 23. Electric field dependence of the index grating formation times of mixtures of the base LC, photoconductive chiral compounds, and TNF measured at 30 °C. (a) 3T-2MB; (b) 3T-2OC; (c) 3T-OXO; (d) 3T-CF3.

#### 4.6.4 Mechanism of the photoconductivity in FLC mixtures

The effect of the electron acceptor (TNF) on the gain coefficient was investigated. As shown in Figure 24, when the concentration of the 3T-2OC was 1 wt%, the magnitude of the gain coefficient increased with the concentration of the TNF.

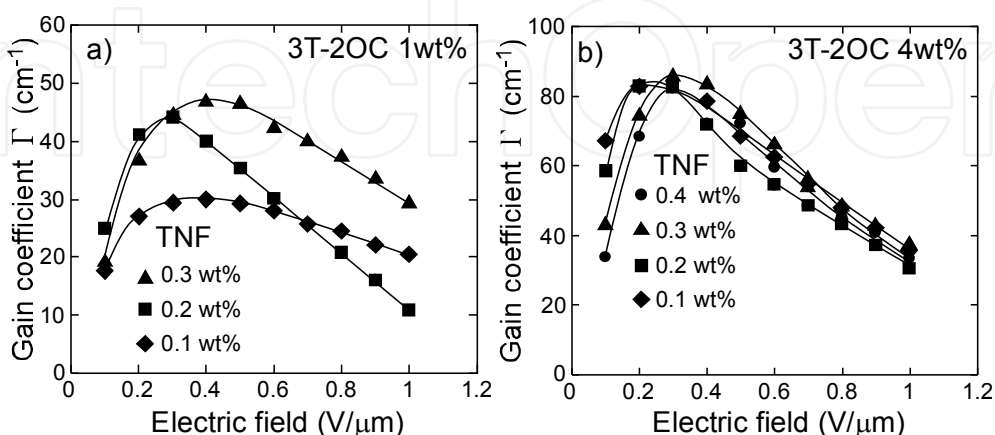


Fig. 24. Dependence of the gain coefficients of the mixture of the base LC, photoconductive chiral compound and TNF on the magnitude of the external electric field. (a) Base LC doped with 1 wt% 3T-2OC; (b) base LC doped with 4 wt% 3T-2OC.

It was considered that the mechanism of the formation of the space-charge field in this case is based on ionic conduction. As discussed in our previous paper, the formation of the space-charge field is based on the difference in the mobilities of the cation and anion generated at the light positions of the interference fringes. A cation of 3T-2OC and an anion of TNF were generated at the interference fringes through photoinduced electron transfer. Both ions drift under the application of an external electric field. The molecular length of 3T-2OC is larger than that of TNF, and thus, the mobility of the 3T-2OC cation is smaller than that of the TNF anion. This difference in mobility is the origin of the charge separation. In this case, the magnitude of the internal electric field is dominated by the concentration of the ionic species. On the other hand, when the concentration of 3T-2OC was 4 wt%, the magnitude of the gain coefficient was independent of the concentration of TNF. Thus, the mechanisms of the formation of the space-charge field are different in the 1 wt% samples and the 4 wt% samples. It was considered that when the concentration of 3T-2OC is high, conduction based on a hopping mechanism occurs. In this case, TNF acts as just the electron acceptor that introduces electron holes into the 3T-2OC molecules.

## 5. Conclusion

The reorientational photorefractive effect based on the response of bulk polarization was observed in dye-doped FLC samples. Photorefractivity was observed only in the ferroelectric phase of these samples, and the refractive index formation time was found to be shorter than that of nematic LCs. The response time was in the order of ms and is dominated by the formation of the internal electric field. These results indicate that the mechanism responsible for refractive index grating formation in FLCs is different from that for non-ferroelectric materials, and is clearly related to the ferroelectric properties of the material. The photorefractivity of FLCs was strongly affected by the properties of the FLCs themselves. Besides properties such as spontaneous polarization, viscosity, and phase transition temperature, the homogeneity of the SS-state was also found to be a major factor. The gain coefficient, refractive index grating formation time (response time) and stability of the two-beam coupling signal were all affected strongly by the homogeneity of the SS-state. Therefore, a highly homogeneous SS-state is necessary to create a photorefractive device. The techniques employed recently in the development of fine LC display panels will be utilized in the future in the fabrication of the photorefractive devices.

## 6. Acknowledgment

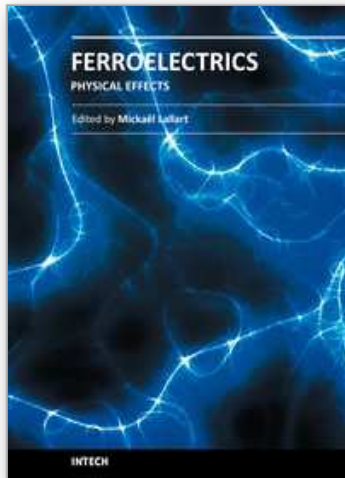
The authors would like to thank the Japan Science and Technology Agency (JST) S-innovation and the Canon Foundation for support.

## 7. References

- Solymar, L.; Webb, J.D.; Grunnet-Jepsen, A. *The Physics and Applications of Photorefractive Materials*; Oxford: New York, 1996.
- Yeh, P. *Introduction to Photorefractive Nonlinear Optics*; John Wiley: New York, 1993.
- Moerner, W. E.; Silence, S. M. *Chem. Rev.* 1994, 94, 127-155.
- Kippelen, B.; Peyghambarian, N. *Advances in Polymer Science, Polymers for Photonics Applications II*, Springer, 2002, 87-156.

- Ostroverkhova, O.; Moerner, W. E. *Chem. Rev.*, 2004, 104, 3267-3314.
- Tay, S.; Blanche, P.A.; Voorakaranam, R.; Tunc, A.V.; Lin, W.; Rokutanda, S.; Gu, T.; Flores, D.; Wang, P.; Li, G.; Hilarie, P.; Thomas, J.; Norwood, R.A.; Yamamoto, M.; Peyghambarian, N. *Nature*, 2008, 451, 694-698.
- Blanche, P.A.; Bablumian, A.; Voorakaranam, R.; Christenson, C.; Lin, W.; Gu, T.; Flores, D.; Wang, P.; Hsieh, W.Y.; Kathaperumal, M.; Rachwal, B.; Siddiqui, O.; Thomas, J.; Norwood, R.A.; Yamamoto, M.; Peyghambarian, N. *Nature*, 2010, 468, 80-83.
- Sasaki, T. *Polymer Journal*, 2005, 37, 797-812.
- Meerholz, K.; Volodin, B.L.; Kippelen, B.; Peyghambarian, N. *Nature* 1994, 371, 497-500.
- Kippelen, B.; Marder, S.R.; Hendrickx, E.; Maldonado, J.L.; Guillemet, G.; Volodin, B.L.; Steele, D.D.; Enami, Y.; Sandalphon; Yao, Y.J.; Wang, J.F.; Röckel, H.; Erskine, L.; Peyghambarian, N. *Science* 1998, 279, 54-56.
- Wiederrecht, G.P.; Yoon, B.A.; Wasielewski, M.R. *Adv. Materials* 2000, 12, 1533-1536.
- Sasaki, T.; Katsuragi, A.; Mochizuki, O.; Nakazawa, Y. *J. Phys. Chem. B*, 2003, 107, 7659-7665.
- Sasaki, T.; Mochizuki, O.; Nakazawa, Y.; Noborio, K. *J. Phys. Chem. B*, 2004, 108, 17083-17088.
- Talarico, M.; Termine, R.; Prus, P.; Barberio, G.; Pucci, D.; Ghedini, M.; Goelemme, A. *Mol. Cryst. Liq. Cryst.*, 2005, 429, 65-76
- Talarico, M.; Goelemme, A. *Nature Mater.*, 2006, 5, 185-188.
- Sasaki, T.; Mochizuki, O.; Nakazawa, N.; Fukunaga, G.; Nakamura, T.; Noborio, K. *Appl. Phys. Lett.*, 2004, 85, 1329-1331.
- Sasaki, T.; Moriya, N.; Iwasaki, Y. *J. Phys. Chem. C*, 2007, 111, 17646-17652.
- Skarp, K.; Handschy, M.A. *Mol. Cryst. Liq. Cryst.* 1988, 165, 439-569.

IntechOpen



## **Ferroelectrics - Physical Effects**

Edited by Dr. Mickaél Lallart

ISBN 978-953-307-453-5

Hard cover, 654 pages

**Publisher** InTech

**Published online** 23, August, 2011

**Published in print edition** August, 2011

Ferroelectric materials have been and still are widely used in many applications, that have moved from sonar towards breakthrough technologies such as memories or optical devices. This book is a part of a four volume collection (covering material aspects, physical effects, characterization and modeling, and applications) and focuses on the underlying mechanisms of ferroelectric materials, including general ferroelectric effect, piezoelectricity, optical properties, and multiferroic and magnetoelectric devices. The aim of this book is to provide an up-to-date review of recent scientific findings and recent advances in the field of ferroelectric systems, allowing a deep understanding of the physical aspect of ferroelectricity.

### **How to reference**

In order to correctly reference this scholarly work, feel free to copy and paste the following:

Takeo Sasaki (2011). Photorefractive Ferroelectric Liquid Crystals, *Ferroelectrics - Physical Effects*, Dr. Mickaél Lallart (Ed.), ISBN: 978-953-307-453-5, InTech, Available from:  
<http://www.intechopen.com/books/ferroelectrics-physical-effects/photorefractive-ferroelectric-liquid-crystals>

**INTECH**  
open science | open minds

### **InTech Europe**

University Campus STeP Ri  
Slavka Krautzeka 83/A  
51000 Rijeka, Croatia  
Phone: +385 (51) 770 447  
Fax: +385 (51) 686 166  
[www.intechopen.com](http://www.intechopen.com)

### **InTech China**

Unit 405, Office Block, Hotel Equatorial Shanghai  
No.65, Yan An Road (West), Shanghai, 200040, China  
中国上海市延安西路65号上海国际贵都大饭店办公楼405单元  
Phone: +86-21-62489820  
Fax: +86-21-62489821

© 2011 The Author(s). Licensee IntechOpen. This chapter is distributed under the terms of the [Creative Commons Attribution-NonCommercial-ShareAlike-3.0 License](#), which permits use, distribution and reproduction for non-commercial purposes, provided the original is properly cited and derivative works building on this content are distributed under the same license.

IntechOpen

IntechOpen